Displacement-Controlled Uniaxial Testing of Metallic, Composite, Polymeric, and Ceramic Specimens

Sabag, Matthew

Section 3458 07/17/2026

***Abstract*—This experiment used an Instron universal testing machine (UTM) to run displacement-controlled tensile and compressive tests on four materials. The specimens were an unknown metal, a biaxial carbon fiber laminate, nylon, and plaster of Paris. This experiment yielded stress-strain diagrams to extract material properties for each one. The metal, carbon fiber, and nylon specimens were tested in tension, while plaster of Paris was tested in compression, and an extensometer was used only for the metal specimen, with crosshead displacement used to estimate strain for the other three. From these graphs, modulus of elasticity, yield strength, ultimate strength, breaking strength, percent elongation, toughness, specific strength, and specific stiffness were found for each specimen. The unknown metal turned out to be ductile, with a modulus of 175.6 GPa, a 0.2% offset yield strength of 412.2 MPa, an ultimate strength of 517.5 MPa, and 24.0% elongation. An uncertainty analysis was run on the specimens, and a power law plastic model fit to the metal gave a strain hardening exponent of 0.121 and a strength coefficient of 767.7 MPa. Comparing these measured properties, along with their uncertainty, against published reference values pointed to the metal being annealed AISI 4130 steel.**

***Index Terms*—Breaking strength, crosshead displacement, displacement-controlled test, extensometer, modulus of elasticity, offset yield strength, percent elongation, power law plastic model, specific strength, specific stiffness, strain hardening, strength coefficient, stress-strain diagram, toughness, ultimate strength.**

I. INTRODUCTION

THE purpose of this experiment was to develop stress-strain diagrams for a range of distinct engineering materials and to demonstrate the use of a universal testing machine (UTM) to perform both tensile and compressive testing. A further objective was to use the resulting mechanical properties to identify the composition of an unknown material tested alongside the others. The specimens tested were an unknown metal, a biaxial carbon fiber laminate, and nylon, all loaded in tension, and plaster of Paris, loaded in compression. The resulting diagrams were used to extract mechanical properties for each specimen, which in turn were compared against published reference values to identify the unknown metal. The remaining three specimens were used to examine and discuss elastic, plastic, and failure behavior across classes of materials.

Testing Apparatus

Displacement-controlled uniaxial testing loads a specimen along a single axis by prescribing the motion of the crosshead, rather than the applied force, until failure occurs. This method was used in place of load-controlled testing, its alternative, for two reasons. First, because the crosshead displacement required to cause failure in these specimens is small, programming the machine to move in small, controlled increments provides a more accurate representation of the resulting stress than would be obtained by imposing load directly. Second, displacement-control avoids the risk of continued force being applied after the specimen has already failed, which under load-control could damage the machine or be unpredictable in nature. UTM components are identified and shown in Fig. 1.

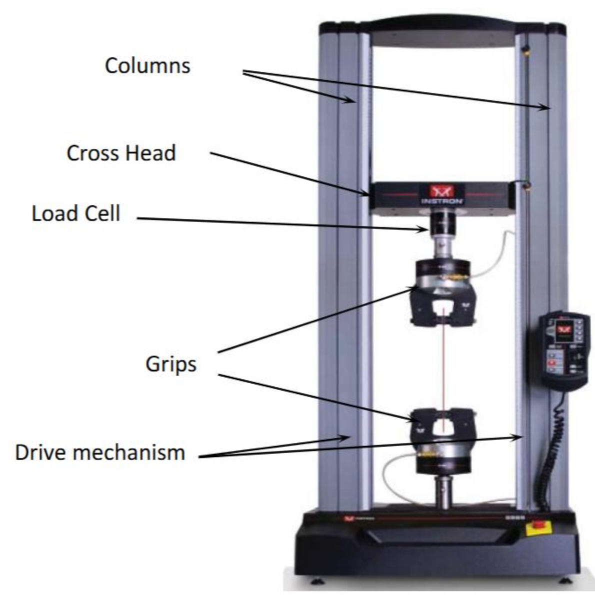

Fig. 1. Describes the components of a Universal Testing Machine, showing the relative location of relevant machine components [11].

The metal and nylon specimens were dog-bone shaped, which concentrated deformation in a narrowed section at the center of the specimen. Without this feature, stress could instead concentrate at the grips, where the specimen is clamped rather than freely deforming in a desired location on the specimen. The biaxial carbon fiber specimen did not use dog-bone geometry. Instead, tabs were bonded to each end and placed in the grips of the UTM to reduce stress concentration at the clamped ends of the specimen within the grips.

An extensometer was used to measure strain directly only for the metal specimen. The extensometer functions only in tension, so it could not be used for the plaster of Paris compression test. It is not applicable to brittle materials such as carbon fiber since it is not usable when the material fractures with no length extension before the material failed. It also cannot be used for the nylon specimen because the strain exceeds roughly 40% of original length that the extensometer is rated to capture. For these three specimens, strain was instead estimated from crosshead displacement.

Stress-Strain Diagrams

Stress, σ, is defined as the internal force, F, acting across a material's cross-sectional area, A. For a specimen under uniaxial stress, this internal force is taken as the load recorded by the UTM's load cell, and the relationship is given by (1).

$$\sigma = \frac{F}{A} \tag{1}$$

Strain, ε, is a unitless measure of a specimen's deformation under load, expressed as the change in length, ΔL, normalized by its initial length prior to loading, L_0, as shown in (2).

$$\varepsilon = \frac{\Delta L}{L_0} \tag{2}$$

This calculation of strain is valid directly when an extensometer is used, since the extensometer measures ΔL across a fixed length mounted directly onto the specimen. The strain data collected is only viable for the unknown metal specimen. In the other samples where an extensometer is not used, ε must instead be calculated from the crosshead displacement of the UTM itself, ΔL, which is not indicative of correct strain measurement from the UTM output. Modeling the machine as a series of springs with a combined stiffness of K_m, its total deflection can be estimated for a given load, P, and subtracted from the total measured displacement from the UTM to approximate the specimen's own elongation, as shown in (3).

$$\varepsilon = \frac{\Delta L - \frac{P}{K_m}}{L_0} \tag{3}$$

Plotting stress against strain produces a stress-strain diagram, which describes material properties independent of the specific size of the specimen tested. At low strains, deformation is elastic, meaning the specimen returns to its original length once the load is removed. Within this region, stress and strain are relatively linear, governed by Hooke's Law, where the slope is the modulus of elasticity, E, a measure of material stiffness. This can be understood clearly from Fig. 2 and (4).

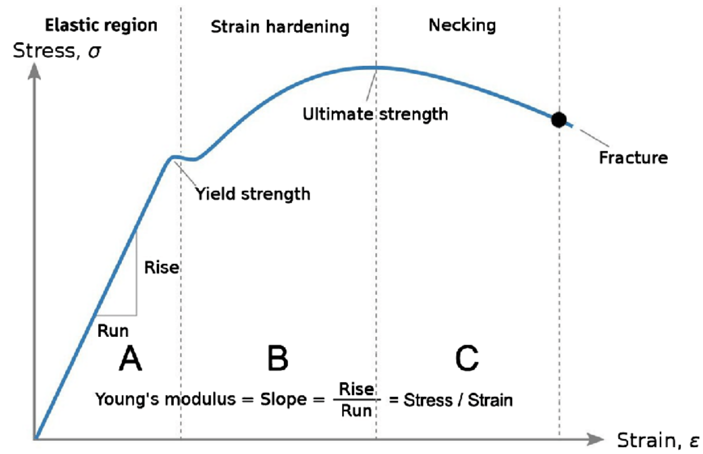

Fig. 2. General stress-strain diagram with labeled key points and regions [6].

$$\sigma = E\varepsilon \tag{4}$$

As loading continues, the specimen reaches its yield point, where deformation becomes plastic, or permanent. Because many materials do not exhibit a single, visually obvious point at which the curve transitions from linear to nonlinear, the yield strength is instead defined using a 0.2% offset method. A parallel line is added alongside the linear-elastic region of the diagram, with slope E, but shifted along the strain axis by a plastic strain of 0.2% (0.002 mm/mm). The stress at which this offset line intersects the measured stress-strain curve is taken as the yield strength, σ_Y, as shown in (5).

$$\sigma_Y = E(\varepsilon - 0.002) \tag{5}$$

Beyond yield, the specimen bears increasing load as the material strain-hardens, up to the ultimate stress, σ_U, the maximum stress the specimen sustains during the test. Past this point, deformation is consistent with a reduction in load-carrying capacity, typically due to necking, until the specimen fractures at the breaking stress, σ_b.

The stress and strain values obtained from (1) and (2) are engineering stress and engineering strain, both of which are calculated using both the specimen's original cross-sectional area and length. This assumption becomes increasingly inaccurate as plastic deformation occurs, since the specimen's actual cross-sectional area decreases via necking and elongates. True stress and true strain instead account for this change by tracking the cross-sectional area of the specimen as it deforms. As long as the assumption that the specimen's volume is conserved during plastic deformation is maintained, both true stress and strain can be expressed as shown in (6) and (7).

$$\sigma_{True} = \sigma_{eng}(1 + \varepsilon_{eng}) \tag{6}$$

$$\varepsilon_{True} = ln(1 + \varepsilon_{eng}) \tag{7}$$

Since both true stress and strain model the material's actual resistance to deformation from the geometric effect of the decreasing cross-section, they were used to develop a plastic material model describing the specimen's post-yield hardening behavior. The elastic component of the true strain, σ_{True}/E , is subtracted from the total true strain to isolate the plastic strain, ε_P. Once this term is accounted for, the relationship between true stress and plastic strain is approximated by the Ramberg-Osgood relationship, shown in (8).

$$\sigma_{True} = K\varepsilon_P^n \tag{8}$$

Here, K is the strength coefficient and n is the strain-hardening exponent. These values are obtained from a linear fit to the log-log plot of true stress versus plastic strain [1]. This model is not applicable in every case. It is generally applicable to annealed materials, but is often a poor fit for brittle materials, which do not exhibit a well-defined plastic hardening region.

Failure Behavior & Material Properties

The result of a material under load differs substantially depending on whether the material is ductile or brittle. Ductile materials, as previously described, exhibit a distinct yield point followed by a region of plastic deformation and strain hardening prior to fracture. Brittle materials, by contrast, exhibit little to no plastic deformation before failure. Their yield point and fracture point are effectively at the same stress, producing a stress-strain curve that remains nearly linear, or only slightly nonlinear, up to the point of sudden failure. Fig. 3 demonstrates fractures of both ductile and brittle materials.

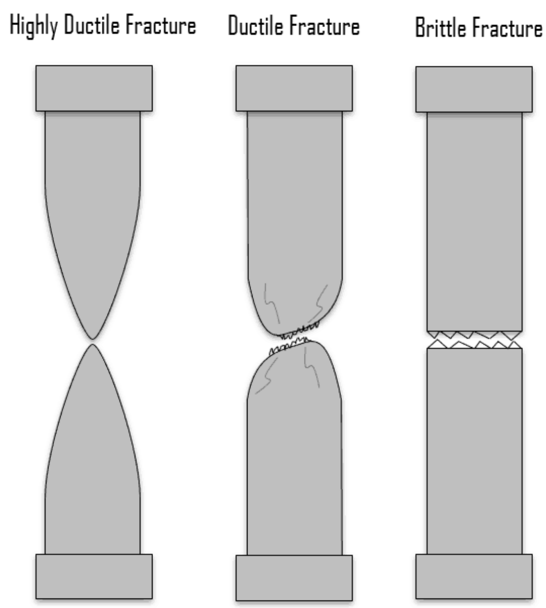

Fig. 3. Visual depiction of ductile and brittle fractures in tension [5].

The way it fails also depends on whether a specimen is loaded in tension or compression. Ductile and brittle failures in tension are discussed above and depicted in Fig. 3. In compression, however, rather than necking, a specimen tends to bulge outward around its circumference or perimeter as it is compressed, generating hoop stresses that prompt the formation and propagation of cracks until the specimen fails. This is the failure type expected for the plaster of Paris specimen, tested here in compression rather than tension.

A material's toughness describes its capacity to absorb energy before it fractures and is obtained by finding the area under the stress-strain curve up to the point of failure. Because stress and strain are recorded as discrete data points rather than a continuous function, this area was evaluated numerically using trapezoidal integration described as the sum for $i = 1$ to $n - 1$, as shown in (9).

$$Toughness = \sum_{i=1}^{n-1} \frac{1}{2}(\sigma_i + \sigma_{i+1})(\varepsilon_{i+1} - \varepsilon_i) \tag{9}$$

However, toughness does not account for a material's weight, which is a critical design consideration in engineering. Specific strength and specific stiffness normalize a material's strength and stiffness by its density, ρ, allowing materials of very different weights to be compared and discussed on as strength- or stiffness-per-unit-mass. The stress used to compute specific strength is the yield stress for ductile materials and the ultimate stress for brittle materials, since these variables are the limiting stress for a system or material. Specific strength and specific stiffness are given by (10) and (11), respectively.

$$\sigma_{Specific} = \frac{\sigma}{\rho} \tag{10}$$

$$E_{Specific} = \frac{E}{\rho} \tag{11}$$

The percent elongation of a specimen is straightforward to obtain. Percent elongation only applies to ductile materials, as brittle materials do not elongate. The operation for calculating percent elongation for ductile materials is shown in (12).

$$Percent\ Elongation = \varepsilon \times 100 \tag{12}$$

II. Procedure

Uniaxial testing was performed on four specimens using an Instron 5967 UTM equipped with a 30 kN load cell, operating in displacement control rather than load control for each test. Prior to testing, the geometry of each specimen was measured and recorded, and those dimensions were used to compute engineering stress from the load data collected by the UTM. For specimens expected to undergo plastic deformation, burnish marks were applied across the narrow gauge section of the dog-bone geometry before testing to allow an independent, physically measured estimate of plastic strain at failure, in addition to the strain estimate obtained from the UTM itself.

Metallic Tensile Specimen

The unknown metal specimen was machined into a dog-bone shape. Its width and thickness were each measured ten times in different locations along the gauge section using a micrometer, from which a mean cross-sectional area and a 95% confidence interval were later established using a student's t-distribution. The specimen was also weighed, and its top surface was imaged alongside a lab ruler for later area estimation using ImageJ [10]. Burnish marks were applied every one inch along the narrow gauge section to establish a reference for measuring plastic elongation post-fracture. The specimen was mounted in the wedge grips of the UTM, and an extensometer was attached and centered about the gauge length to measure strain directly throughout the test. A constant crosshead displacement rate of 7 mm/min was applied until the specimen fractured. After testing, the specimen was pieced together, and the deformed length of the section containing the fracture was measured directly and later compared to the original length.

Carbon Fiber Tensile Specimen

The biaxial carbon fiber specimen geometry was measured once, rather than with repeated statistical sampling, since the cross-sectional area was uniform along its length. Its thickness and width were recorded with a micrometer over the section between the tabbed grip ends. Because the carbon fiber laminate was expected to fail in a brittle manner, no burnish marks were applied. The specimen was mounted in the UTM grips, and because the extensometer is unsuitable for brittle specimens expected to fracture with little-to-no warning, strain was instead estimated from the crosshead displacement. The associated strain was normalized by the initial length of the gauge section between the grips. A constant crosshead displacement rate of 7 mm/min was applied until fracture.

Nylon Tensile Specimen

The nylon specimen, molded into a dog-bone shape like the carbon fiber specimen, was measured for thickness and width using a micrometer. As with the metal specimen, burnish marks were applied every one inch along the gauge section prior to testing to allow plastic elongation at failure to be measured directly after fracture. Because the nylon specimen was expected to undergo elongation exceeding the extensometer's rated travel range, strain was instead estimated from the crosshead displacement by normalized by the specimen's initial gauge length. The crosshead was initially displaced at 7 mm/min and after one minute once the load response had stabilized, the crosshead speed was increased to 80 mm/min to continue the test through to failure within a reasonable timeframe. After fracture, the specimen was reassembled. The section with the fracture was originally two inches, the length of two burnish marks. The deformed length of this section was measured directly afterwards to manually obtain geometry for percent elongation calculations.

Plaster of Paris Compressive Specimen

The plaster of Paris specimen, cast into a cylindrical shape, had its diameter and height measured with calipers prior to testing. No burnish marks were applied, since the specimen was expected to fail in a brittle manner with negligible plastic deformation. The specimen was placed between the compression plates of the UTM. Since the extensometer is not compatible with compressive loading, strain was estimated from the crosshead displacement and normalized by the specimen's initial height, just as the carbon fiber and nylon specimens. A constant crosshead displacement rate of 0.5 mm/min was applied until the specimen's load-carrying capacity had visibly and permanently deformed through cracking along its height and progressive crushing.

All load, displacement, and strain data recorded by the UTM were exported and compiled for each specimen. These data, together with the geometric measurements taken prior to testing, were subsequently used to generate engineering stress-strain diagrams for all four specimens, allowing for the presentation of results.

III. Results

Stress and strain were acquired from the raw load, displacement, and strain data recorded for each of the four specimens, using the cross-sectional area and gauge length measured before any tests were conducted. A table of relevant measured and calculated values, along with the corresponding stress-strain diagram, is presented below for the unknown metal, carbon fiber, nylon, and plaster of Paris specimens.

Unknown Metal

Table I shows the ten measurements of length and width of the dog-bone shaped gauge section of the specimen, along with the average of the values.

Table I
Unknown Metal Repeated Measurements

Reference	Width (mm)	Thickness (mm)
1	11.12 ± 0.001	1.60 ± 0.001
2	11.12 ± 0.001	1.59 ± 0.001
3	11.12 ± 0.001	1.60 ± 0.001
4	11.07 ± 0.001	1.59 ± 0.001
5	11.07 ± 0.001	1.59 ± 0.001
6	11.09 ± 0.001	1.58 ± 0.001
7	11.06 ± 0.001	1.59 ± 0.001
8	11.12 ± 0.001	1.58 ± 0.001
9	11.10 ± 0.001	1.59 ± 0.001
10	11.12 ± 0.001	1.58 ± 0.001
Average	11.099 ± 0.04	1.589 ± 0.04

Table II lists the cross-sectional area, gauge length, modulus of elasticity, yield strength, 0.2% offset yield strength, ultimate strength, breaking strength, percent elongation by last strain reading, percent elongation by burnished marks, toughness, specific strength, specific stiffness, and density for the unknown metal specimen. The area was calculated from the average width and thickness measurements taken across the ten measurements. The modulus was calculated from the slope of the linear elastic portion of the curve, and both the offset yield strength and the ultimate and breaking strengths were read directly from the stress-strain data. Percent elongation is reported using both the final strain reading from the extensometer and the physically measured burnished marks. Toughness was calculated using the area under the stress-strain curve up until the fracture point, and both the specific strength and specific stiffness were each calculated from these values alongside the specimen's density.

Table II
Unknown Metal Geometry & Material Properties

Dimension or Property	Value
A_c	17.63 ± 0.36 mm²
L_{gauge}	6.3 ± 0.05 cm
E	175.6 ± 6.3 GPa
σ_Y	244.1 ± 3.3 MPa
σ_Y (0.2% $offset$)	412.2 ± 5.0 MPa
σ_U	517.5 ± 4.7 MPa
σ_b	396.1 ± 6.6 MPa
$\%\ Elongation\ (Strain)$	22.9% ± 0.6%
$\%\ Elongation\ (Burnish)$	24.0% ± 0.33%
$Toughness$	112.9 ± 4.4 MJ/m³
$\sigma_{Specific}$	52.5 ± 4.5 MPa·cm³/g
$E_{Specific}$	22,370 ± 85.2 MPa·cm³/g
ρ	7.87 ± 0.21 g/cm³

Fig. 4 shows the engineering stress-strain curve generated for the unknown metal specimen from the extensometer strain data and the corresponding load readings. The curve shows a linear region at low strain, followed by a yielding region and an extended leveled region where stress increases only gradually with strain. Past this flat portion, the curve reaches its highest point before beginning a slow decline as strain continues to increase toward fracture. The plot has been cut off at the point of fracture, since data collected afterward reflects the machine and grips rather than the specimen itself.

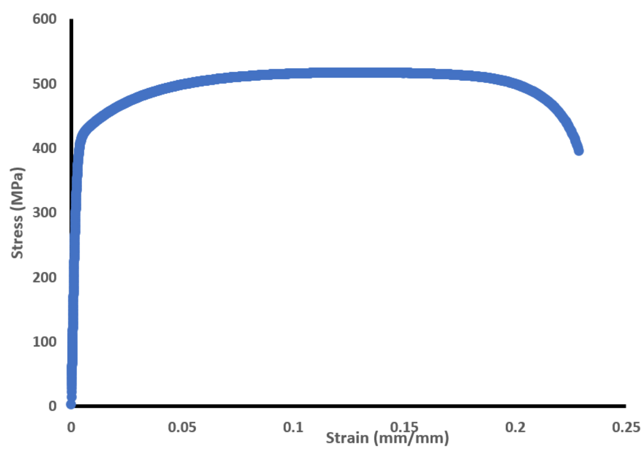

Fig. 4. Unknown metal specimen's related stress-strain diagram.

Carbon Fiber

Table III lists the cross-sectional area, gauge length, modulus of elasticity, ultimate strength, breaking strength, toughness, specific strength, specific stiffness, and density for the carbon fiber specimen. The area was calculated from a single width and single thickness measurement taken between the tabbed grip sections, and the gauge length corresponds to the distance between the grips. The modulus was calculated from the slope of the curve at low strain, where the stress-strain plot remains linear, and the ultimate and breaking strengths are reported as the same value, since fracture occurred suddenly at the highest recorded stress. Due to the nature of the carbon fiber material, yielding is not exhibited in the diagram and thus excluded from the table and not reported. It is true for all brittle materials that they do not yield.

Table III
Carbon Fiber Geometry & Material Properties

Dimension or Property*	Value
A_c	21.4 ± 0.36 mm²
L_{gauge}	305 ± 0.5 mm
E	29.1 ± 1.6 GPa
σ_U	990.2 ± 16.3 MPa
σ_b	990.2 ± 16.3 MPa
$Toughness$	10.0 ± 3.4 MJ/m³
$\sigma_{Specific}$	687.6 ± 12.8 MPa·cm³/g
$E_{Specific}$	20,240 ± 157.0 MPa·cm³/g
ρ	1.44 ± 0.13 g/cm³

*Yield strength and percent elongation are omitted for this specimen because carbon fiber is a brittle material.

Fig. 5 shows the stress-strain curve generated for the carbon fiber specimen using strain estimated from the crosshead displacement and the corresponding load readings. The curve shows a line with an increasing slope from the start of loading through to fracture. This diagram lacks any clear point where it shifts from linear to nonlinear. The curve ends suddenly at its highest point where the specimen simultaneously fractured. As with the metal specimen, data recorded after this point has also been excluded from the plot. The plot exhibits mild nonlinear trends, which does not allow for the determination of some material properties for the carbon fiber specimen.

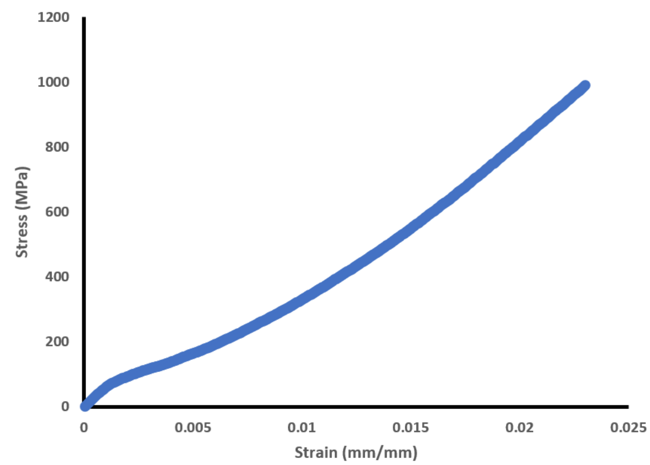

Fig. 5. Carbon fiber specimen's related stress-strain diagram.

Nylon

Table IV lists the cross-sectional area, gauge length, modulus of elasticity, 0.2% offset yield strength, ultimate strength, breaking strength, percent elongation by last strain reading, percent elongation by burnished marks, toughness, specific strength, specific stiffness, and density for the nylon specimen. The area was calculated from a single width and single thickness measurement. The modulus, offset yield strength, ultimate strength, and breaking strength were each obtained from the stress-strain curve generated using the crosshead-based strain calculation. Percent elongation is again reported using both the last strain reading and the burnished marks method, alongside the evaluated toughness, and specific strength and stiffness that are both obtained by dividing each respective property by material density.

Table IV
Nylon Geometry & Material Properties

Dimension or Property	Value
A_c	37.1 ± 0.36 mm²
L_{gauge}	91 ± 0.5 mm
E	1.34 ± 0.41 GPa
σ_Y (0.2% $offset$)	22.5 ± 2.5 MPa
σ_U	29.36 ± 6.1 MPa
σ_b	12.65 ± 3.8 MPa
$\%\ Elongation\ (Strain)$	60.4% ± 5.6
$\%\ Elongation\ (Burnish)$	71.9% ± 8.1
$Toughness$	13.4 ± 1.6 MJ/m³
$\sigma_{Specific}$	8.65 ± 0.87 MPa·cm³/g
$E_{Specific}$	959 ± 33.9 MPa·cm³/g
ρ	1.15 ± 0.43 g/cm³

Fig. 6 shows the engineering stress-strain curve generated for the nylon specimen using strain estimated from the crosshead displacement and the corresponding load readings. The curve rises through an early linear region before reaching a local peak, followed by a relatively flat region. Once the nylon specimen reaches a local yield point, a narrow neck starts to form somewhere along the gauge section, and the stress drops slightly as that region deforms faster than the rest of the specimen. As the gauge section material strain hardens, the curve suddenly spikes up, then is accompanied by a gradual decline until fracture occurs at the far right of the plot. It is also worth noting that the feed rate during this specimen's testing was changed for the sake of time. To stay consistent with the other specimens and to maintain a clear, legible graph, the data has been cut off at the point of fracture.

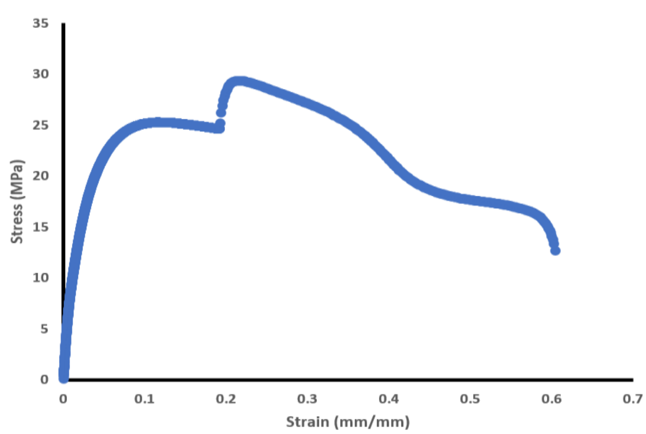

Fig. 6. Nylon specimen's related stress-strain diagram.

Plaster of Paris

Table V lists the cross-sectional area, height, modulus of elasticity, ultimate strength, toughness, specific strength, specific stiffness, and density for the plaster of Paris specimen. The area was calculated from the measured diameter of the cylindrical specimen, and the height corresponds to the length of the specimen before compression testing. The modulus was calculated from the slope of the beginning, linear portion of the curve. Although the specimen experienced the crushing stress and cracked, the ultimate strength is reported as the highest stress recorded during the test.

Table V
Plaster of Paris Geometry & Material Properties

Dimension or Property*	Value
A_c	506.3 ± 22.4 mm²
h	53.85 ± 0.5 mm
E	0.79 ± 0.19 GPa
σ_U	7.08 ± 1.2 MPa
$Toughness$	0.061 ± 0.009 MJ/m³
$\sigma_{Specific}$	5.76 ± 0.14 MPa·cm³/g
$E_{Specific}$	642 ± 28.2 MPa·cm³/g
ρ	1.2 ± 0.1 g/cm³

*Yield strength and percent elongation are omitted for this specimen because plaster of Paris is a brittle material.

Fig. 7 shows the stress-strain curve generated for the plaster of Paris specimen using the crosshead-displacement estimated strain and the associated load. The noisiness of the graph comes from brittle crushing of the specimen. The data for the plot has not been cut off since the specimen continued to carry load through progressive crushing.

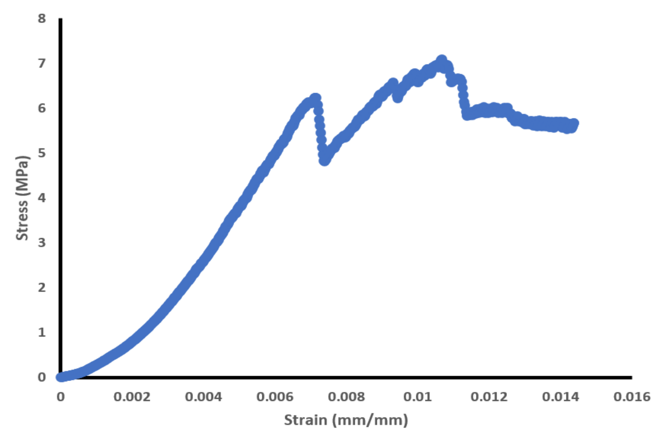

Fig. 7. Plaster of Paris specimen's related stress-strain diagram.

IV. Discussion

The stress-strain diagrams and calculated properties presented in Section III are examined below to explain the observed elastic, plastic, and failure behavior of each specimen, identify the composition of the unknown metal, and compare the material properties of the four specimens tested. Presented below in Table VI are the summarized material property values calculated for the four distinct materials.

Table VI
Summarized Material Properties per Specimen

Property	Units	Unknown Metal	Carbon Fiber	Nylon	Plaster of Paris
Modulus of Elasticity	GPa	175.6 ± 6.3	29.1 ± 1.6	1.34 ± 0.41	0.79 ± 0.19
Yield Strength	GPa	244.1 ± 3.3	-	16.8 ± 3.7	-
Yield Strength (0.2% offset)	MPa	412.2 ± 5.0	-	22.5 ± 2.5	-
Ultimate Strength	MPa	517.5 ± 4.7	990.2 ± 16.3	29.36 ± 6.1	7.08 ± 1.2
Breaking Strength	MPa	396.1 ± 6.6	990.2 ± 16.3	12.65 ± 3.8	7.08 ± 1.2

Table VI
Summarized Material Properties per Specimen Continued

Property	Units	Unknown Metal	Carbon Fiber	Nylon	Plaster of Paris
% Elongation (last strain reading)	-	22.9% ± 0.6	-	60.4% ± 5.6	-
% Elongation (burnished marks)	-	24.0% ± 0.33	-	71.9% ± 8.1	-
Toughness	MJ/m³	112.9 ± 4.4	10.0 ± 3.4	13.4 ± 1.6	0.061 ± 0.009
Specific Strength	MPa·cm³/g	52.5 ± 4.5	687.6 ± 12.8	8.65 ± 0.87	5.76 ± 0.14
Specific Stiffness	MPa·cm³/g	22,370 ± 85.2	20,240 ± 157.0	959 ± 33.9	642 ± 28.2
Density	g/cm³	7.87 ± 0.21	1.44 ± 0.13	1.15 ± 0.43	1.2 ± 0.1

Interpretation of Elastic, Plastic, and Failure Behavior

The unknown metal specimen demonstrated typical failure behavior associated with a ductile metal, with a clear linear elastic region followed by yielding, a strain hardening plateau, and a gradual decline in stress associated with necking right before fracture. The similarity between the two measured percent elongation values supports the reliability of both the extensometer reading and the physically measured burnished marks. The carbon fiber specimen instead showed a mildly nonlinear, stiffening trend that ended abruptly at the highest recorded stress. This was followed by a sudden, brittle fracture with no advance warning, although there were audible moments of weaker fibers failing. The nylon specimen showed an early yield point followed by a decreasing plateau, then a sudden spiking stress, and finally consistent decrease in stress until failure. This is a shape associated with polymer chains progressively aligning with the direction at which load is applied, making the material more resistant to deformation, before the material ultimately fractures. The plaster of Paris specimen loaded approximately linearly before dropping sharply from crushing and continuing to carry noisy residual stress, consistent with a brittle material crushing internally.

Failure Surfaces

For the unknown metal, the fracture surface shows the cup and cone shape typical of ductile necking failure, more consistent with a higher ductility material. For the carbon fiber specimen, individual fibers are fractured at different locations along the failure plane, consistent with the breaking of fibers of varying local strength, one after the other. For the nylon specimen, the degree of necking is extensive immediately before fracture, consistent with the large elongation recorded in Table IV. For the plaster of Paris specimen, the failure surface shows vertical cracking and slight outward bulging consistent with hoop stress crushing, rather than a single fracture along the cross-sectional area of the specimen. Each of the failure surfaces for the specimens are consistent with the expectation set before the experiment was conducted.

Identification of the Unknown Metal

The uncertainty analysis performed for the unknown metal specimen results in a propagated uncertainty of approximately 0.60% in the reported stress values. The uncertainty in strain, taken from the manufacturer accuracy of the extensometer itself, is approximately 0.5% of the reading. This level of stress and strain uncertainty is small enough to be considered negligible next to the spread in published property values across similar candidate metals, since differences between competing steel grades typically span tens of megapascals or more, far exceeding what a fraction of a percent could explain. Using the measured density, modulus of elasticity, yield strength, ultimate strength, and percent elongation of the unknown metal, the material was compared against a published reference for annealed AISI 4130 steel, summarized in Table VII.

Table VII
Comparison of Unknown Metal Properties Against Annealed AISI 4130

Property	Units	Unknown Metal	Annealed AISI 4130 Steel [4]
E	GPa	175.6 ± 6.3	190-205 ± 5.0
$\sigma_Y\ (2\%\ offset)$	MPa	412.2 ± 5.0	460 ± 10.0
σ_U	MPa	517.5 ± 4.7	530 ± 10.0
$\%\ Elongation\ (Burnish)$	-	24.0% ± 0.33	22% ± 2.0
ρ	g/cm³	7.87 ± 0.21	7.85 ± 0.25

As shown in Table VII, the unknown metal is most consistent with annealed AISI 4130 steel. The measured ultimate strength of 517.5 ± 4.7 MPa falls within about 2.4% of the reference value of 530 ± 10.0 MPa, the measured percent elongation of 24.0% ± 0.33 falls within 2 percentage points of the reference value of 22% ± 2.0, and the measured density of 7.87 ± 0.21 g/cm³ matches the reference value of 7.85 ± 0.25 g/cm³ almost exactly. The measured modulus of elasticity, 175.6 ± 6.3 GPa, falls below the reference range of 190 to 205 ± 5.0 GPa by approximately 8 to 15%. This lower difference remains the same for the measured 0.2% offset yield strength of 412.2 ± 5.0 MPa also falling below its reference value of 460 ± 10.0 MPa by approximately 10%. This makes logical sense because the 0.2% offset relies on the measured modulus to define the slope of the offset line. A modulus that is measured slightly lower with respect to the true value produces an offset line that is also lower than that value. This means that the offset line will intersect the stress-strain curve at a lower stress than the specimen's actual yield point.

The measured uncertainty in stress, approximately 0.60%, is the smallest difference between AISI 4130 and the unknown metal and is smaller than any of the other candidate steels considered. No other researched steel types matched as closely across all five properties as annealed AISI 4130 steel. This shows that the steel identification process was not carelessly executed by comparing the unknown metal between two similar alloys but rather reflects the best fit to one specific steel choice. However, a single tensile test does not produce enough information to certainly differentiate the chosen steel, annealed

AISI 4130, from other Cr-Mo alloy steels that have similar composition and treatments. This is because their published property values can overlap with one another. Additional testing, such as hardness testing or chemical composition analysis will yield more definitive results about the unknown metal's exact composition and grade.

Extensometer vs. Crosshead Displacement

The extensometer should be used whenever a specimen's expected elongation remains within the rated range of the device, since it measures deformation directly on the specimen's gauge section. The measured modulus of elasticity for nylon, 1.34 ± 0.41 GPa, and the measured 0.2% offset yield strength, 22.5 ± 2.5 MPa, both fall below the handbook modulus and yield strength of approximately 3.2 to 3.5 GPa and 80 to 90 MPa, respectively, for the same material [14]. This large disagreement is explained by grip slack accumulating over the nylon specimen's long gauge length. Deflection in the grips and frame is measured in the same direction, or in series, with the specimen when strain is estimated from crosshead displacement. This additional non-material deflection of the instrumentation is more impactful when considering small strains than it is later in the test when the strains become insignificantly larger. For similar reasons, the extensometer remains unusable for the carbon fiber and plaster of Paris specimens, since it cannot be used in compression, and is not appropriate for a specimen expected to fracture with little-to-no warning, in a brittle manner.

Specific Strength and Specific Stiffness

Based on the values reported in Table VI, the carbon fiber specimen exhibited the highest specific strength of 687.6 ± 12.8 MPa·cm³/g, while the unknown metal specimen exhibited the highest specific stiffness of 22,370 ± 85.2 MPa·cm³/g. The carbon fiber laminate specimen is expected to exhibit the greatest specific strength because of the nature of the material. The fibers are positioned parallel to the direction in which the uniaxial load is applied, creating immense stress in tension within the specimen. As for the specific strength, the ultimate stress experienced by the carbon fiber, which is also the breaking stress, was normalized by the density of the material. The methodology in which the density was obtained is outlined in the previous sections. With regards to the highest specific stiffness, the unknown metal specimen's nonlinear modulus makes its specific stiffness dependent on the density obtained and which portion of the associated stress-strain graph is used to deduce the modulus of elasticity.

Plastic Material Model

The power law fit to the true stress and plastic strain data for the unknown metal specimen gave a strain hardening exponent of 0.121 and a strength coefficient of 767.7 MPa, with a coefficient of determination of 0.941. This exponent falls within the range expected for an annealed metal [13]. This type of plastic model was not applied to the carbon fiber or plaster of Paris specimens, since both are brittle and did not have a clear plastic region. It was also not applied to the nylon specimen, because the model itself is a poor fit for nylon's actual deformation behavior. The Hollomon relationship assumes a roughly uniform and volume-conserving plastic deformation within the gauge section, applicable to the unknown metal's gradual strain hardening and necking. The nylon specimen deformed through cold drawing, where a neck formed early and then propagated along the gauge length.

V. Conclusion

This experiment used an Instron UTM to run displacement controlled tensile and compressive tests on four materials, an unknown metal, a biaxial carbon fiber laminate, nylon, and plaster of Paris, and the resulting data was used to build stress-strain diagrams for each one. The unknown metal turned out to be ductile, with a modulus of 175.6 GPa, a 0.2% offset yield strength of 412.2 MPa, an ultimate strength of 517.5 MPa, and 24.0% elongation. Comparing these values against a published reference indicated that the metal was annealed AISI 4130 steel. The carbon fiber and plaster of Paris specimens both broke in a brittle way with no clear yield point, while nylon stretched substantially before breaking, reaching 71.9% elongation. Out of all four materials, carbon fiber had the highest specific strength, and the unknown metal had the highest specific stiffness. The uncertainty analysis on the metal specimen showed that the geometry measurements were the main source of error. A power law model fit to the metal's plastic region gave a strain hardening exponent of 0.121 and a coefficient of determination of 0.941, showing a reasonably good fit.

Appendix

Variable Uncertainties

Every propagated uncertainty in this analysis begins with the resolution or manufacturer accuracy of the instrument used to collect a measurement. Table VIII lists the uncertainty used for each direct measurement used in this analysis, along with the instrument that was utilized for that measurement.

Table VIII
Instrument Uncertainties

Variable	Uncertainty	Method
Width	± 0.001 mm	Micrometer [13]
Thickness	± 0.001 mm	Micrometer [13]
Load	± 0.5%	Instron [2]
Strain	± 0.5%	Extensometer [3]
Mass	± 0.0005 N	Digital Lab Scale [13]
Length	± 0.02 mm	Caliper [13]
Length	± 0.5 mm	Ruler [13]

Student's T-Distribution & Confidence Interval

Because only ten width and thickness readings were taken for the unknown metal specimen, a student's t-distribution was used rather than typical standard deviation, since this small sample size requires a wider interval to achieve a 95% confidence interval. The sample standard deviation was calculated first, shown in (13), followed by the resulting confidence interval, shown in (14).

$$S_X = \sqrt{\frac{\sum_{i=1}^{n}(X_i - \bar{x})^2}{n-1}} \quad (13)$$

$$CI = \bar{x} \pm t \times \frac{S_X}{\sqrt{n}} \quad (14)$$

Monte Carlo Uncertainty for Young's Modulus

The uncertainty in the modulus of elasticity was estimated using a Monte Carlo simulation since modulus is derived from the slope of a linear function rather than propagated uncertainty of variables. A small number of points were selected from the linear elastic region of the stress-strain, each with an uncertainty propagated from the load and area uncertainties. A simulated dataset was generated, and a line of best fit was calculated for that simulated dataset. This process was repeated until the modulus uncertainty could be taken as the standard deviation of the simulated sample and scaled to a 95% confidence interval by being multiplied by two, shown in (15).

$$\mu_E = 2 \times \sigma_{MC} \quad (15)$$

RSS Propagation

The remaining uncertainties in this analysis, including cross-sectional area, stress, density, specific strength, and specific stiffness, were each propagated using the root sum square (RSS) method, which combines the uncertainty of two or more independent variables into the uncertainty of a quantity derived from them. Each subsection below gives the specific RSS relationship used for that quantity.

RSS Cross-Sectional Area

$$\mu_{A_C}^2 = \frac{\partial A_C^2}{\partial w^2}\mu_w^2 + \frac{\partial A_C^2}{\partial t^2}\mu_t^2 \quad (16)$$

RSS Stress

$$\mu_\sigma^2 = \frac{\partial \sigma^2}{\partial P^2}\mu_P^2 + \frac{\partial \sigma^2}{\partial A_C^2}\mu_{Ac}^2 \quad (17)$$

RSS % El.

$$\mu_{\%\,El.}^2 = \frac{\partial \%\,El.^2}{\partial L_f^2}\mu_{L_f}^2 + \frac{\partial \%\,El.^2}{\partial L_i^2}\mu_{L_i}^2 \quad (18)$$

RSS Density

$$\mu_\rho^2 = \frac{\partial \rho^2}{\partial m^2}\mu_m^2 + \frac{\partial \rho^2}{\partial V^2}\mu_V^2 \quad (19)$$

RSS Specific Strength

$$\mu_{\sigma_{Specific}}^2 = \frac{\partial \sigma_{specific}^2}{\partial \sigma^2}\mu_\sigma^2 + \frac{\partial \sigma_{specific}^2}{\partial \rho^2}\mu_\rho^2 \quad (20)$$

RSS Specific Stiffness

$$\mu_{E_{Specific}}^2 = \frac{\partial E_{specific}^2}{\partial E^2}\mu_E^2 + \frac{\partial E_{specific}^2}{\partial \rho^2}\mu_\rho^2 \quad (21)$$

References

[1] CAEflow, "Ramberg-Osgood Stress-Strain Relationship." [Online]. Available: https://caeflow.com/fea/ramberg-osgood-stress-strain/

[2] "2580 Series Static Load Cells Data Sheet," Instron.com. [Online]. Available: https://www.instron.com/wp-content/uploads/2024/07/2580-series-load-cells-1.pdf

[3] "2630-100 Series Clip-On Extensometer Reference Manual," Instron.com. [Online]. Available: https://www.instron.com/wp-content/uploads/2024/07/2630-100-series-clip-on-extensometer-reference-manual.pdf

[4] MakeItFrom, "Annealed 4130 Cr-Mo Steel." [Online]. Available: https://www.makeitfrom.com/material-properties/Annealed-4130-Cr-Mo-Steel

[5] Nuclear Power, "Fracture of Material, Fracture Mechanics." [Online]. Available: https://www.nuclear-power.com/nuclear-engineering/materials-science/material-properties/toughness/fracture-of-material-fracture-mechanics/

[6] ResearchGate, "A Typical Stress-Strain Curve." [Online]. Available: https://www.researchgate.net/figure/A-typical-stress-strain-curve-5_fig1_348780093

[7] S. Ridgeway, "Lab 3 Discussion," Gainesville, FL: 2026, unpublished.

[8] S. Ridgeway, "Lab 3 Discussion Details," Gainesville, FL: 2026, unpublished.

[9] S. Ridgeway, "Lab 3 Displacement Controlled Uniaxial Testing Assignment," Gainesville, FL: 2026, unpublished.

[10] S. Ridgeway, "General Procedures for Calculating Area via Image, Mechanics of Materials Laboratory," Gainesville, FL: 2026, unpublished.

[11] S. Ridgeway, "Lab 3 Intro_Background," Gainesville, FL: 2026, unpublished.

[12] S. Ridgeway, "Lab 3 Procedure," Gainesville, FL: 2026, unpublished.

[13] S. Ridgeway, "Lab 2 Uncertainty," Gainesville, FL: 2025, unpublished.

[14] G. Subhash and S. Ridgeway, Mechanics of Materials Laboratory Course, Synthesis SEM Lectures on Experimental Mechanics, San Rafael, CA: Morgan & Claypool Publishers, 2018.